RSC Advances

PAPER

View Article Online
View Journal | View Issue

Cite this: *RSC Adv.*, 2022, **12**, 24101

A novel SERS substrate of MIL-100(Fe)/AgNFs for sensitive detection of ascorbic acid in cellular media†

Wang Qiao,[ab] Yiran Wang,[ab] Zhenxia Zhao,[a] Yujiao Wang,[b] Kui Chen,[b] Zhongxing Zhao*[a] and Min Li*[b]

Received 5th July 2022
Accepted 16th August 2022

DOI: 10.1039/d2ra04146d

rsc.li/rsc-advances

A novel SERS substrate of MIL-100(Fe)/AgNFs was firstly prepared for sensitive and selective detection of ascorbic acid (L-AA), with a LOD of 10^{-11} M. A spectral decrease of MIL-100(Fe)/AgNFs towards L-AA solution thanks to the efficient capture and reduction of Fe^{3+} in MIL-100(Fe) constituted the assay, which was demonstrated to function well in food samples and in cellular media for L-AA sensing.

Introduction

Ascorbic acid (L-AA), also known as vitamin C, is an important nutrient but cannot be synthesized in humans. The source of vitamin C intake mainly comes from vegetables, fruits or medicines.[1] It plays key roles in many physiological processes and in modulating neurological diseases due to its good antioxidant properties.[2–5] For example, L-AA is released extracellularly to scavenge reactive oxygen species (ROS) so as to protect brain cells from oxidative damage.[6,7] It shows not only effective prevention and protection from many neurological diseases caused by brain damage, but also active in the treatment of scurvy benefiting from its neuro modulatory functions. Excessive or low expression of L-AA in the body will be an indicative message of disorders of some biological functions or appearance of neurological diseases. Therefore, it is of great importance to quickly monitor the concentration of ascorbic acid in cells or in the physiological media with high sensitivity and accuracy. Even though several methods have been established for L-AA detection, such as electrochemistry with a limit of detection (LOD) of 10^{-8}–10^{-9} M,[8,9] high performance liquid chromatography (HPLC) for determination of L-AA in foods,[10] chemiluminescence[11] and fluorescence which realize 10^{-7} M for L-AA sensing,[12,13] limitations related to low sensitivity, poor specificity, expensive equipment requirements and time-consuming sample procedures, are still existing. New strategies for the detection of L-AA with high sensitivity, specificity and simplicity are thus highly desirable.

Surface-Enhanced Raman Scattering (SERS), as an emerging powerful spectroscopic technique with ultrasensitive and label free features, has been widely used in many fields such as chemicals detection,[14] biomolecules sensing,[15] food additives monitoring[16] and so on.[17,18] The function of SERS-based sensor mainly relies on the electromagnetic field enhancement mechanism (EM), where the coupled surface plasmon resonances can enhance the Raman scattering of the target molecules by up to 10^{11}.[19] In this case, the key step is to construct the sandwich-type structures of noble metal nanoparticles and to trap the molecules of interest sitting or binding in the nanogap between particles, which adds much tedious and complex work to the experiments. In addition, the multi-step strategy will reduce the efficiency and accuracy of SERS technique. Another possibility for Raman scattering enhancing is the chemical enhancement mechanism (CM), which is usually closely related to the charge transfer resonance (CT) between the frontier orbital of the adsorbed molecule and the Fermi level of the metal substrate.[20] Using SERS technology, the detection limit of L-AA could realize 10^{-8}–10^{-9} M.[20–23] Ag or Au was usually used as the SERS substrate in these research, and the detection sensitivity and specific recognition to L-AA need to be improved.

Metal–organic frameworks (MOFs) can be regarded as a high density, atomically dispersed metal topological skeleton,[24] which facilitates and increases the efficiency of its interaction with the target molecules involving the applications in catalysis,[25,26] and chemical detection.[27] Combining the MOF materials which confines and concentrates target molecules with the metal nanoparticles which serve as a conventional SERS-active substrate will thus be an efficient way to sensing molecules of interest. Wu[28] *et al.* integrated AuNPs onto NH_2-UiO-66(Zr) for sensing orange II dyes in food samples. The detection limit was 0.4 mg L^{-1} which is far beyond than that of MOFs or AuNPs

[a]*School of Chemistry and Chemical Engineering, Guangxi Key Laboratory of Agro-Environment and Agro-Product Safety, Guangxi University, Nanning 530004, China*

[b]*CAS Key Laboratory for Biomedical Effects of Nanomaterials and Nanosafety, Institute of High Energy Physics, Chinese Academy of Sciences, Beijing 100049, China. E-mail: limin/ihep.ac.cn*

† Electronic supplementary information (ESI) available. See https://doi.org/10.1039/d2ra04146d

alone. Shao[29] *et al.* reduced Ag^{+} to Ag on MIL-101(Cr) substrate and reached 10^{-11} M for 4-ATP detection.

Our previous work[27] has demonstrated that MIL-100(Fe) presents high SERS activity and can be an excellent substrate in VOCs detection *via* CM. *In situ* synthesizing MIL-100(Fe) on a SERS-active silver-island film (AgNFs), might further enhance the Raman intensity of target molecules through both EM and CM processes. Employing MIL-100(Fe)/AgNFs as the substrate and utilizing the pronounced redox properties of L-AA to Fe^{3+}, this approach reached a LOD of 10^{-11} M for L-AA sensing, much lower than the conventional methods.

Results and discussion

Scheme 1 showed the synthetic route of the preparation of MIL-100(Fe)/AgNFs at room temperature (RT), and the experimental details were provided in the experimental section of SI. Briefly, a silver nanofilm was grown on the glass wafer and followed by covering an ultrathin film of gold *via* ion spraying. Then mercaptopropionic acid (MPA) was linked to the substrate *via* Au–S bonding. After reacting with Fe^{3+} and 1,3,5-benzenetricarboxylic acid (H_3BTC) for 24 h, the composite MIL-100(Fe)/AgNFs was obtained.

Fig. 1a displayed the typical SEM image of MIL-100(Fe). It could be seen that MIL-100(Fe) presented both bulk and flake crystals and was uniformly fixed and dispersed on AgNFs surface through the exposed carboxyl groups. The XRD patterns of glass, AgNFs and MIL-100(Fe)/AgNFs were shown in Fig. 1b. Glass presents a broad diffraction hump, which is a typical characteristic peak of inorganic glass materials.[30] The diffraction peaks at 38.3° observed for AgNFs/glass corresponds to Ag (111),[31] proving the successful synthesis of AgNFs on glass. Furthermore, after *in situ* growth of MIL-100(Fe) on AgNFs, the characteristic peaks of MIL-100(Fe) appeared, consisting with the reported result.[32] This proved that the crystals grown on AgNFs were MIL-100(Fe). The grown process of MIL-100(Fe)/AgNFs was characterized *via* SEM and presented in Fig. S1.† It was clearly seen that only a little amount of MIL-100(Fe) was observed to occupy on AgNFs surface at 12 h accompanying with the exposure of most silver nanoparticles. With time extension, MIL-100(Fe) gradually covered AgNFs surface and after 24 h clumps of materials appeared on the surface (Fig. S1f†). The morphology of *in situ* synthesized MIL-100(Fe) in solution instead on AgNFs surface was also presented in Fig. S2,† which

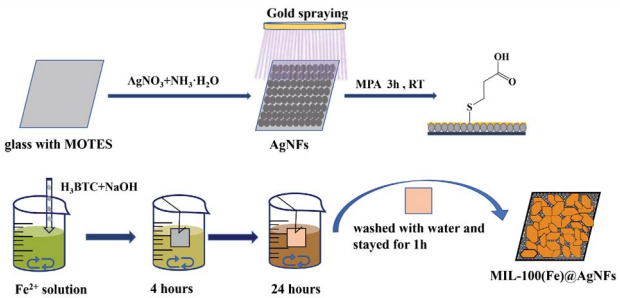

Scheme 1 Synthetic route for MIL-100(Fe)/AgNFs preparation at RT.

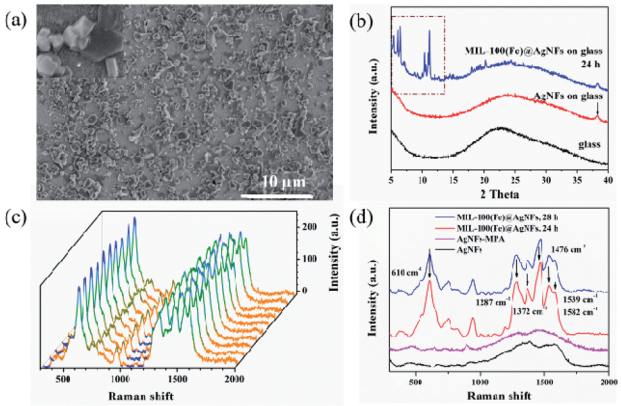

Fig. 1 (a) SEM of MIL-100(Fe)/AgNFs grown for 24 hours. (b) XRD of glass, AgNFs and MIL-100(Fe)/AgNFs on glass. (c) Random Raman spectra of MIL-100(Fe)/AgNFs at ten different spots. (d) Raman spectra of AgNFs, AgNFs modified with MPA, MIL-100(Fe) growing for 24 h and 28 h, respectively, on AgNFs.

was observed to be similar to that obtained *via* hydrothermal synthesis method.[33] Comparing Fig. S1f† with Fig. S2,† it was safe to conclude that MIL-100(Fe) tended to grow in the way of in solution after 24 h. Fig. S3† showed that the XRD peaks of MIL-100(Fe) became to be entirety when it grew to 12 h and the peak intensity reached a plateau at 24 h, indicating again that the formation of MIL-100(Fe) on AgNFs basically completed at 24 h. Notedly, the Raman spectra in Fig. 1d showed the intensity of MIL-100(Fe)/AgNFs for 24 h growth was higher than that for 28 h. The Raman scattering generated by MIL-100(Fe)/H_2O interface might be destroyed to some extent by the covered clumps of materials which however contributes very little to the scattering. Besides, a slight oxidation of AgNFs may also account for the decrease of Raman intensity of MIL-100(Fe)/AgNFs for 28 h growth. The formation of MIL-100(Fe) on AgNFs was further confirmed by the EDS characterization (Fig. S4†). Fe element was expected to be less proportional than Au and Ag and was observed to distribute evenly throughout the materials. Taken together, these results demonstrated the successful synthesis of MIL-100(Fe)/AgNFs.

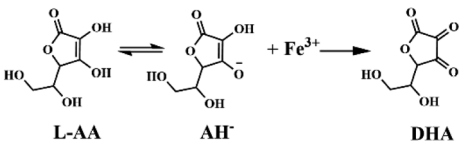

(1)

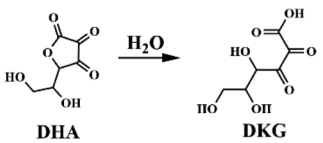

(2)

The size of MIL-100(Fe) crystals was determined to be 200–400 nm for 24 h growth. Different from the topography of MIL-100(Fe) obtained through hydrothermal synthesis method,[33,34]

some crystals grown on the surface exhibited the crystal structure in lamelliform with less stacking and vertical growth (inset in Fig. 1a and S3†). That is, MIL-100(Fe) in flake shape possibly possessed more defections, which could expose more Fe^{3+} active sites and consequently facilitating its reaction with L-AA in the next step.

L-AA exhibited strong reduction and chelation with metal ions, making it an effective nonheme iron adsorbent. In a weakly acidic environment, L-AA actively underwent a redox reaction with Fe^{3+} as indicated in eqn (1). During this process, L-AA was oxidized to dehydroascorbic acid (DHA), while only a very small part of DHA could converted to 2,3-diketogulonic acid (DKG) (eqn (2)) according to the literature.[35,36] In this experiment, MIL-100(Fe) effectively enriched L-AA from solution and promoted the reduction of L-AA to Fe^{3+} in MIL-100(Fe), resulting in the structure destruction. Spectral changes in MIL-100(Fe) upon L-AA chelating and reducing Fe^{3+} constitutes the assay, finally realizing the detection of L-AA in real samples and cellular media.

Considering that acidic environment would facilitate the redox reaction of L-AA to Fe^{3+}, it was necessary to explore the effect of pH values and reaction time of L-AA to MIL-100(Fe)/AgNFs to obtain the optimized conditions and ensure the sensing validity of this assay. To remove the interference from AgNFs due to its oxidation in the system containing NaOH and Fe^{2+}, a thin film of gold was sputtered on AgNFs for protection. The sputtering details were provided in SI and the results were shown in Fig. 2 and S5.† The optimized sputtering parameters was determined to be 5 mA for 30 s as indicated in Fig. 2b.

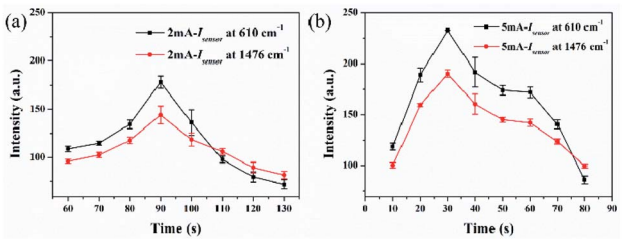

Fig. 2 The relationship of I_{610} and I_{1476} for MIL-100(Fe)/AgNFs with gold spraying time under (a) 2 mA, (b) 5 mA, respectively.

The typical Raman spectra of MIL-100(Fe)/AgNFs were shown in Fig. 1c. The peak appeared at 610 cm^{-1} was corresponding to the out-of-plane deformation modes of the C–H bond. The peaks at 1582 cm^{-1} are from the in-plane vibrations of the benzene rings, while the peaks at 1287, 1372, 1476 and 1539 cm^{-1} are more likely to the vibrations of C=O or C–O group.[27,37] Taking the intensity of the peak at 610 cm^{-1} (I_{610}) as the reference, the relationship of the intensity change ΔI_{610} of MIL-100(Fe)/AgNFs *versus* various pH conditions was tested. It clearly showed that the stable pH window for MIL-100(Fe)/AgNFs was in the range of 5.0–7.0 (Fig. 3a–c). When being exposed to L-AA with certain concentration (10^{-8} M), the intensity of MIL-100(Fe) decreased expectedly as presented in Fig. 3d and e. The tendency of ΔI_{610} with pH variations was shown in Fig. 3f. It was clearly seen that I_{610} decreased rapidly at the pH range of 4.0–8.0 due to the efficient redox reaction of ascorbic acid with Fe^{3+}.

Based on the determined stable reaction window as well as the reduction efficiency of L-AA to Fe^{3+} indicated in Fig. 3c and f, pH 5.0 seemed to be a reasonable choice. Considering the final pH of the solution for MIL-100(Fe) synthesis on AgNFs is 5.2, it is fair to tune the pH of the detection system to 5.2 to ensure both the stability and sensing efficiency of MIL-100 (Fe)/AgNFs to L-AA.

A clear time dependency was observed for I_{610} when exposure MIL-100(Fe)/AgNFs to L-AA with concentrations of 10^{-5} M and 10^{-8} M, respectively, as shown in Fig. 4. For both cases, the

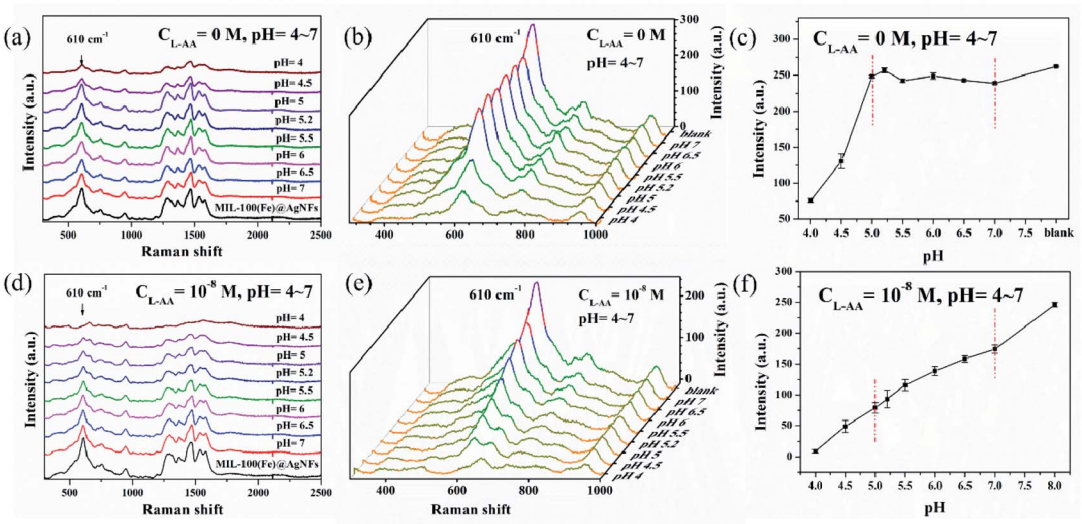

Fig. 3 SERS spectra of MIL-100(Fe)/AgNFs in the absence (a) and in the presence (d) of L-AA at different pH aqueous solution. (b) and (e) Details of the spectra at 300 cm^{-1} to 1000 cm^{-1}. (c) The stable window of MIL-100(Fe)/AgNFs at various pH environments. (f) The reaction efficiency of MIL-100(Fe)/AgNFs with 10^{-8} M L-AA at various pH environments.

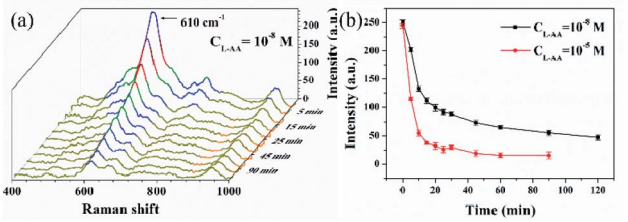

Fig. 4 (a) SERS spectra of MIL-100(Fe)/AgNFs upon 10^{-8} M of L-AA for different reaction time at 610 cm^{-1}. (b) Intensity decrease of MIL-100(Fe)/AgNFs at 610 cm^{-1} upon L-AA of different concentrations with reaction time.

Raman intensity of MIL-100(Fe) showed a rapid decrease within 10 min, suggesting a fast Fe^{3+} chelating and reducing process. It is expectable to observe a faster intensity decrease for higher L-AA concentration. The reaction equilibrium of this reaction system reached at around 30 min as indicated in Fig. 4c. Considering the time-efficient requirement for a sensor, 30 min was selected and considered enough for this sensing system.

To assess the sensing performance of MIL-100(Fe)/AgNFs to L-AA, SERS spectra were collected after exposure MIL-100(Fe)/AgNFs to L-AA with various concentrations (10^{-13} M to 10^{-5} M). With increasing concentration of L-AA, pronounced decrease of I_{610} was observed including the intensity of the bands at 1287 cm^{-1} (νC=O and νC–O), 1476 cm^{-1} (νC=O), 1538 cm^{-1} (νC=O) and 1582 cm^{-1} (νC=C). Importantly, the intensity decrease ($\Delta I_{610}/I_0$) was found to be quantitatively correlated to the concentration of L-AA as shown in Fig. 5b (R^2 = 0.995, from 10^{-11} M to 10^{-6} M), with a detection limit of 10^{-11} M. The results showed that the SERS spectra of MIL-100(Fe)/AgNFs can be used to quantitatively detect L-AA in aqueous solution. In order to prove the sensing performance of this platform for real samples, vitamin C lozenges and fruits were selected and the results were shown in Fig. 5b. Since the L-AA content in effervescent tablet has been indicated (marked on the bottle), so it is easy to prepare the effervescent tablet samples with determined concentration of L-AA. From Fig. 5c, it was clearly seen that the results for L-AA sensing in effervescent tablet samples matched greatly to the working plot (the red columns) at three decided concentrations, and the recovery of L-AA ($C_{detection}/C_{preparation}$) was determined to be 97.8%, 98.8% and 104.8% from low to high concentrations respectively. Three orange samples with approximate concentrations according to the rough content level of L-AA in an orange (1.82×10^{-7} M) were prepared and the detection results were presented in Fig. 5b. The detected concentrations of the orange samples after 10×, 100× and 1000× dilution were 1.54×10^{-8} M, 1.64×10^{-9} M and 2.77×10^{-10} M respectively, through the fitted equation of the linear working plot ($y = 0.093x + 1.173$, Fig. 5b). The detection results for the food samples proved the sensing accuracy of MIL-100(Fe)/AgNFs platform for L-AA.

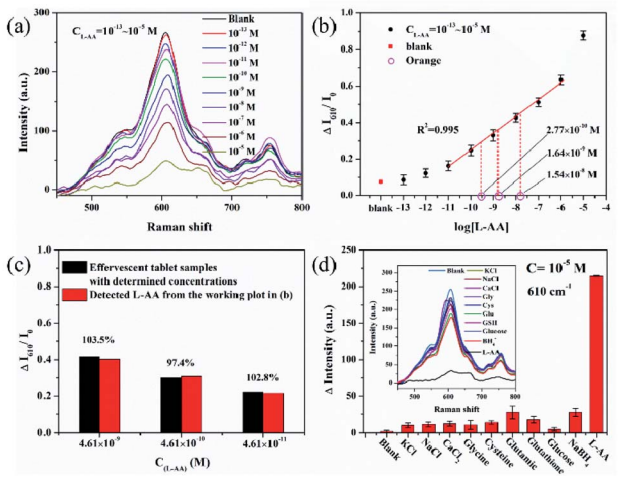

Fig. 5 (a) Spectra change MIL-100(Fe)/AgNFs at 610 cm^{-1} upon L-AA with various concentrations. (b) $\Delta I_{610}/I_0$ as a function of L-AA concentrations. I_0 means the initial intensity of MIL-100(Fe)/AgNFs before reacting with L-AA. Error bars indicate three parallel samples, each with 5 measurements. (c) The recovery of L-AA in effervescent tablets to the extracted values from the working plot in (b). (d) Intensity changes of MIL-100(Fe)/AgNFs when exposure to 10^{-5} M solutions of interfering substances in aqueous solutions at pH 5.2.

Considering the existence of L-AA in complex biological environment, the specificity investigation of MIL-100 (Fe)/AgNFs is thus of necessity especially in the applications in cellular media. The specificity to L-AA was evaluated by comparing the SERS spectra after exposure to 10^{-5} M aqueous solution of the interfering substances including K(I), Na(I), Ca(II), Cl^-, BH_4^-, glycine (Gly), cysteine (Cys), glutamic acid (Glu), glutathione (GSH) and glucose as shown in Fig. 5d. Among those, BH_4^-, Glu and GSH were selected as the reducing substances similar to L-AA to verify if these substances had effect on the reduction of Fe^{3+}. The results showed that all these interfering substances had very subtle spectra change, confirming the selectivity of MIL-100(Fe)/AgNFs to L-AA detection. It should be noted that with the framework decomposition of MIL-100 to more and more L-AA, the chemical environment of C–H (610 cm^{-1}) on the benzene ring changed and resulted in the band shift as shown in Fig. 5a and d.[38] However, this shift would not contribute to the change in signal intensity. Compared with other interfering substances, the spectra changes of the reducing ones are slightly larger, but far less than the responses of L-AA.[39,40] This might be due to the enol structure of L-AA, which facilitated its binding to Fe^{3+} in MIL-100(Fe) in acidic environment. A distinct change only occurred in case of exposure to L-AA, indicating the interference coming from other additives including the reducing substances was negligible.

The assay's sensing capability of its potential applications in the cellular medium might be more important. L-AA solutions with different concentrations were spiked into the lytic 4T1 cells (mouse breast cancer cells, ESI† for details). Fig. 6a showed the peak intensity ($\Delta I_{610}/I_0$) gradually decreased with increasing L-AA concentrations. A good linear relationship between $\Delta I_{610}/I_0$ and the log(L-AA) was obtained (R^2 = 0.989, from 10^{-11} M to 10^{-6} M). The LOD was determined to keep at 10^{-11} M, indicating that the interference from the cell components was minimal. To further demonstrate the potential applications of this platform in cells, the detection of lysates of 4T1 and B16

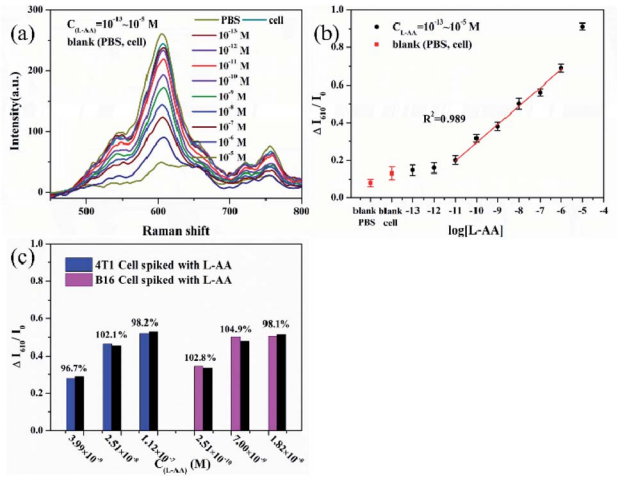

Fig. 6 (a) Spectral changes of MIL-100(Fe)/AgNFs at 610 cm^{-1} upon L-AA with various concentrations spiked in 4T1 cells. (b) $\Delta I_{610}/I_0$ as a function of L-AA concentrations spiked in 4T1 cells. (c) The recovery of spiked L-AA in 4T1 and B16 cells to the extracted values from the working plot in (b).

(melanoma cell) spiked with L-AA solution with different concentrations, respectively, were performed. Fig. 6b showed the detection results of both L-AA spiked cells were well matching to the working plot, which proves that the sensor possesses great potential for clinical sample detection with high sensitivity and quantitation.

Conclusions

A novel SERS sensing platform was developed for L-AA detection by chelating and reducing Fe^{3+} in MIL-100(Fe). A spectral decrease of MIL-100(Fe)/AgNFs was utilized to quantify the concentration of L-AA, which could attribute to the decomposition of MIL-100(Fe) during the redox process. This sensing platform combined both the enrichment capacity of MIL-100(Fe) and the outstanding Raman enhancement of AgNFs, which drove it to 10 picomolar sensitivity and high specificity over other interferences for L-AA detection. The assay presented its sensitivity and selectivity in vitamin C lozenges and fruit samples. Finally, the sensitive detection of L-AA in 4T1 and B16 was also successfully demonstrated. To the best of our knowledge, this is the first report on chemicals sensing by utilizing the structural decomposition of MOF. This work provides a possibility for rapid and sensitive detection of some neurochemicals in assisting the clinical diagnosis by using SERS spectroscopy.

Conflicts of interest

There are no conflicts to declare.

Acknowledgements

This work was supported by the National Natural Science Foundation of China (Grant No. 22074147) and the National Basic Research Program of China (No. 2019YFB1309703).

Notes and references

1 K. A. Naidu, *Nurture*, 2003, **2**, 7.
2 F. E. Harrison and J. M. May, *Free Radical Biol. Med.*, 2009, **46**, 719.
3 L. Chen, X. Sun, Z. Wang, Y. Lu, M. Chen, Y. He, H. Xu and L. Zheng, *Clin. Nutr.*, 2021, **40**, 5327.
4 M. Agathocleous, C. E. Meacham, R. J. Burgess, E. Piskounova, Z. Zhao, G. M. Crane and S. J. Morrison, *Nature*, 2017, **549**, 476.
5 S. J. Ballaz and G. V. Rebec, *Pharmacol. Res.*, 2019, **146**, 104321.
6 B. Brahma, R. E. Forman, E. E. Stewart, C. Nicholson and M. E. Rice, *J. Neurochem.*, 2000, **74**, 1263.
7 R. Siushansian, S. J. Dixon and J. X. Wilson, *J. Neurochem.*, 1996, **66**, 1227.
8 S. I. Kaya, S. Kurbanoglu and S. A. Ozkan, *Crit. Rev. Anal. Chem.*, 2019, **49**, 101.
9 N. Tukimin, J. Abdullah and Y. Sulaiman, *J. Electrochem. Soc.*, 2018, **165**, B258.
10 V. Spinola, E. J. Llorent-Martinez and P. C. Castilho, *J. Chromatogr. A*, 2014, **1369**, 2.
11 C. Wang, M. I. Halawa, B. Lou, W. Gao, J. Li and G. Xu, *Analyst*, 2021, **146**, 1981.
12 Y. Wang, Y. Yang, W. Liu, F. Ding, P. Zou, X. Wang, Q. Zhao and H. Rao, *Mikrochim. Acta*, 2019, **186**, 246.
13 H. Rao, H. Ge, Z. Lu, W. Liu, Z. Chen, Z. Zhang, X. Wang, P. Zou, Y. Wang, H. He and X. Zeng, *Microchim. Acta*, 2016, **183**, 1651.
14 S. Schlucker, *Angew. Chem., Int. Ed. Engl.*, 2014, **53**, 4756.
15 G. Balakrishnan, G. V. Barnett, S. R. Kar and T. K. Das, *Anal. Chem.*, 2018, **90**, 6959.
16 J. Fu, H. Lai, Z. Zhang and G. Li, *Anal. Chim. Acta*, 2021, **1161**, 338464.
17 H. Chen, S. G. Park, N. Choi, J. I. Moon, H. Dang, A. Das, S. Lee, D. G. Kim, L. Chen and J. Choo, *Biosens. Bioelectron.*, 2020, **167**, 112496.
18 L. Cheng, Z. Zhang, D. Zuo, W. Zhu, J. Zhang, Q. Zeng, D. Yang, M. Li and Y. Zhao, *ACS Appl. Mater. Interfaces*, 2018, **10**, 34869.
19 Y. Kalachyova, D. Mares, V. Jerabek, P. Ulbrich, L. Lapcak, V. Svorcik and O. Lyutakov, *J. Phys. Chem. C*, 2017, **19**, 14761.
20 J. R. Lombardi and R. L. Birke, *J. Phys. Chem. C*, 2014, **118**, 11120.
21 J. L. Cholula-Diaz, D. Lomeli-Marroquin, B. Pramanick, A. Nieto-Arguello, L. A. Cantu-Castillo and H. Hwang, *Colloids Surf., B*, 2018, **163**, 329.
22 I. B. Ansah, W.-C. Lee, C. Mun, J.-J. Rha, H. S. Jung, M. Kang, S.-G. Park and D.-H. Kim, *Sens. Actuators, B*, 2022, **353**, 131196.
23 M. R. El-Zahry, I. H. Refaat, H. A. Mohamed and B. Lendl, *Anal. Bioanal. Chem.*, 2016, **408**, 4733–4741.
24 Q. L. Zhu and Q. Xu, *Chem. Soc. Rev.*, 2014, **43**, 5468.
25 D. Wang, M. Wang and Z. Li, *ACS Catal.*, 2015, **5**, 6852.
26 K. G. Laurier, F. Vermoortele, R. Ameloot, D. E. De Vos, J. Hofkens and M. B. Roeffaers, *J. Am. Chem. Soc.*, 2013, **135**, 14488.

27 J. H. Fu, Z. Zhong, D. Xie, Y. J. Guo, D. X. Kong, Z. X. Zhao, Z. X. Zhao and M. Li, *Angew. Chem., Int. Ed.*, 2020, **59**, 20489.
28 L. Wu, H. Pu, L. Huang and D. W. Sun, *Food Chem.*, 2020, **328**, 127105.
29 Q. Shao, D. Zhang, C.-e. Wang, Z. Tang, M. Zou, X. Yang, H. Gong, Z. Yu, S. Jin and P. Liang, *J. Phys. Chem. C*, 2021, **125**, 7297.
30 E. Kleebusch, C. Patzig, T. Höche and C. Rüssel, *J. Mater. Sci.*, 2016, **51**, 10127.
31 J. D. Liu, Z. W. Liu, Z. Q. Chen, H. J. Zhang and B. J. Ye, *Appl. Surf. Sci.*, 2019, **496**, 143527.
32 K. Guesh, C. A. D. Caiuby, Á. Mayoral, M. Díaz-García, I. Díaz and M. Sanchez-Sanchez, *Cryst. Growth Des.*, 2017, **17**, 1806.
33 S.-H. Huo and X.-P. Yan, *J. Mater. Chem.*, 2012, **22**, 7449.
34 H. Lv, H. Zhao, T. Cao, L. Qian, Y. Wang and G. Zhao, *J. Mol. Catal. A: Chem.*, 2015, **400**, 81.
35 J. Shen, P. T. Griffiths, S. J. Campbell, B. Utinger, M. Kalberer and S. E. Paulson, *Sci. Rep.*, 2021, **11**, 7417.
36 A. Mlakar, A. Batna, A. Dudda and G. Spiteller, *Free Radical Res.*, 1996, **25**, 525.
37 J.-G. Lee, B. N. Joshi, E. Samuel, S. An, M. T. Swihart, J. S. Lee, Y. K. Hwang, J.-S. Chang and S. S. Yoon, *J. Alloys Compd.*, 2017, **722**, 996.
38 W. Zhu, J. H. Hutchison, M. Dong and M. Li, *ACS Sens.*, 2021, **6**, 1704.
39 Y. Huang, N. He, Q. Kang, D. Shen, X. Wang, Y. Wang and L. Chen, *Analyst*, 2019, **144**, 6609.
40 X. Gao, X. Zhou, Y. Ma, T. Qian, C. Wang and F. Chu, *Appl. Surf. Sci.*, 2019, **469**, 911.